RADIATION RESEARCH **158**, 505–515 (2002)
0033-7587/02 $5.00

Enhanced Values of the RBE and H Ratio for Cytogenetic Effects Induced by Secondary Electrons from an X-Irradiated Gold Surface

D. Regulla,[a,1] E. Schmid,[b] W. Friedland,[a] W. Panzer,[a] U. Heinzmann[c] and D. Harder[d]

[a] *Institute of Radiation Protection,* [b] *Institute of Radiation Biology, and* [c] *Institute of Pathology, GSF—National Research Center for Environment and Health, 85764 Neuherberg, Germany; and* [d] *Prof. em. of Medical Physics and Biophysics, Georg-August-University, 37075 Göttingen, Germany*

Regulla, D., Schmid, E., Friedland, W., Panzer, W., Heinzmann, U. and Harder, D. Enhanced Values of the RBE and H Ratio for Cytogenetic Effects Induced by Secondary Electrons from an X-Irradiated Gold Surface. *Radiat. Res.* 158, 505–515 (2002).

The low-energy secondary electrons emerging from the entrance surface of an X-irradiated gold foil increase the dose to cells in contact with or at micrometer distances from this surface (*Radiat. Res.* 150, 92–100, 1998). We examined the effect of the spectrum of these low-energy electrons on the RBE for cytogenetic effects and showed that this RBE was increased. A monolayer of surface-attached human T lymphocytes was exposed to 60 kV X rays in the absence or presence of a gold foil positioned immediately behind the cell layer or separated from it by a Mylar foil 0.9 or 2 μm thick. The enhancement of dose in the cell nuclei caused by the photoelectrons and Auger electrons emerging from the entrance surface of the gold foil was measured by TSEE dosimetry. Dose enhancement factors of 55.7, 46.6 and 37.5 were obtained with 0, 0.9 and 2 μm of Mylar inserted between the gold surface and the cell layer. This large enhancement results from the photoelectric effect in the gold foil, as shown by the accompanying Monte Carlo calculations of the secondary electron spectra at the gold surface. Auger electrons from the gold foil generally were not able to penetrate into the cell nuclei except for that fraction of the cells that had a very thin (< 0.7 μm) layer of cytoplasm and membranes between gold surface and cell nucleus. The dose–yield curves for dicentric chromosomes plus centric rings and for acentric fragments obtained after exposures without or with the gold foil were linear-quadratic. The coefficient α, the slope of the linear yield component, was increased in the presence of the gold foil and showed RBE values ranging from 1.7 to 2.2 compared to exposures in absence of the gold foil. The ratio of the yield of interstitial deletions and dicentrics (H ratio) was significantly increased from about 0.17 in the absence of the gold foil to about 0.22 in the presence of the gold foil. The increases in the RBE and the H ratio are interpreted in microdosimetric terms: The preferred occurrence of electron track ends in the vicinity of the gold surface causes an increase in the dose-mean restricted linear energy transfer in cell nuclei exposed to the photoelectrons and Auger electrons.

INTRODUCTION

The composition of the human body normally comprises various interfaces between materials with different atomic number *Z*, e.g. between the soft tissues as typical low-*Z* materials and the bones and teeth as materials with higher atomic numbers. Further low-*Z* /high-*Z* interfaces may have been introduced artificially, such as the surfaces of metallic implants and the interfaces between X-ray contrast media containing iodine compounds and the blood cells or blood vessel walls. If such inhomogeneous media are exposed to X rays with photon energies in the diagnostic range, the photoelectric effect causes the release of photoelectrons and Auger electrons within the high-*Z* material. As a result of a combination of convection (spatial shift in the direction of flight) and scattering, some of these secondary electrons emerge from the high-*Z* region into the low-*Z* medium, causing a large increase in absorbed dose over the value obtained in the absence of the high-*Z* material. This dose enhancement can cover two orders of magnitude, but because of the limited range of the emerging secondary electrons, it remains spatially confined to a single or a few cell layers lining the high-*Z* material surface. Several studies of this effect have been published (*1–3*). The classical example of this interface effect is that of red bone marrow cells lining the trabeculae of the substantia spongiosa in the skeleton, so that local dose enhancement is contributing to the risk of hemopoietic malignancies (*4*). However, the dose enhancement in cells adjacent to bone surfaces could also have relevance for the induction of malignant bone tumors, as one may assume regarding the effects of α particles from bone-seeking radionuclides on bone-lining cells (*5, 6*).

We have previously demonstrated an enhancement of absorbed dose due to photoelectrons and Auger electrons emerging from X-irradiated material interfaces by physical dosimetry and by applying ''biological dosimeters'' (*1, 3*). But beyond dose enhancement there is a spectral effect: These secondary electrons will be more or less slowed

[1] Author to whom correspondence should be addressed at GSF-National Research Center for Environment and Health, P.O. Box 1129, 85764 Neuherberg, Germany; e-mail: regulla@gsf.de.

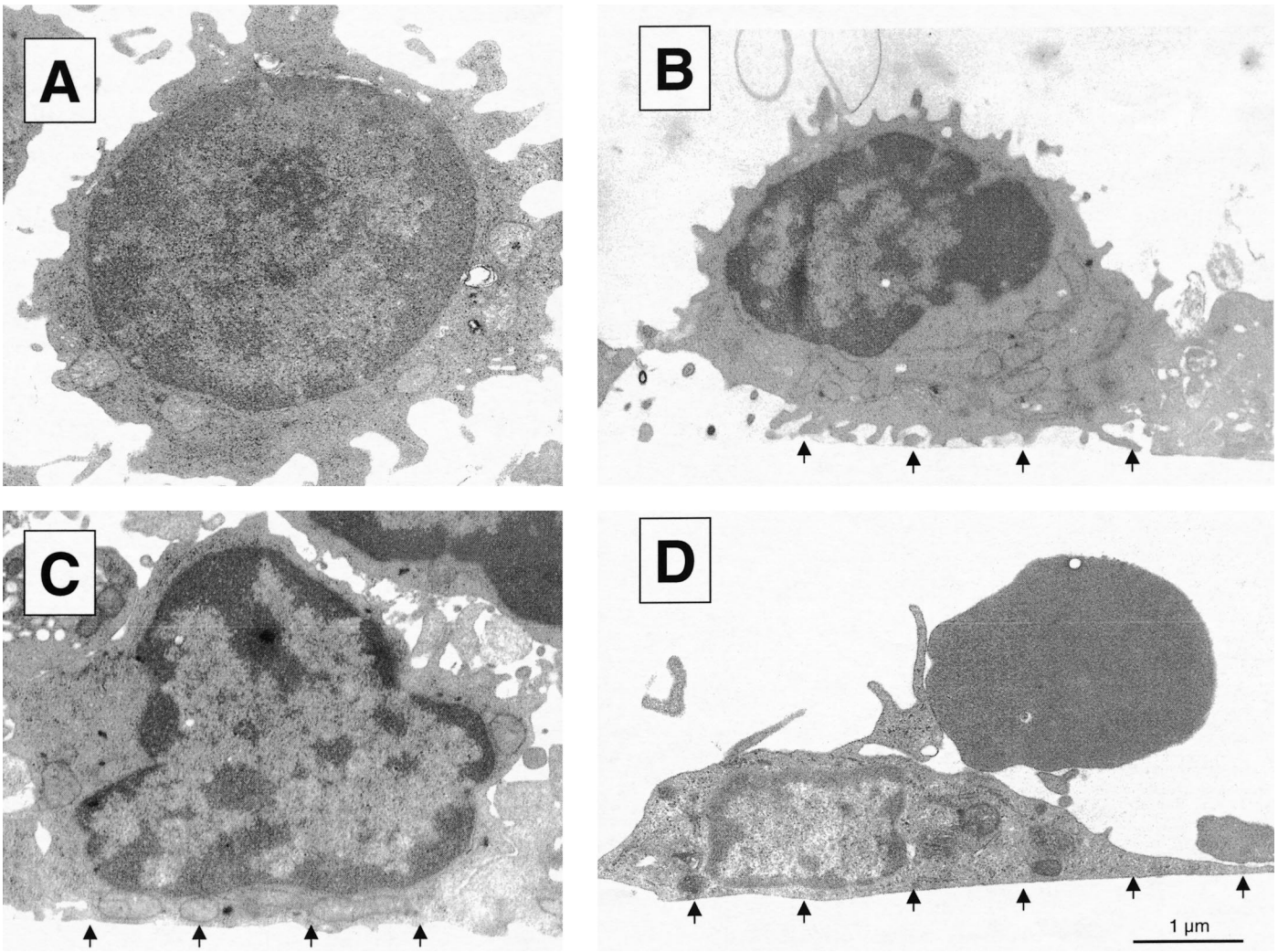

FIG. 1. Electron micrographs of human T lymphocytes, stimulated with phytohemagglutinin, in more or less close contact with the Mylar foil bottom of the culture dishes. Panel A shows a lymphocyte with a regular round nucleus, not attached to the foil. Panel B: The microvilli of a lymphocyte are in contact with the foil; the arrows indicate the surface plane of the foil. Panel C: The surface structures of a lymphocyte directly attached to the foil are smoothed. Panel D: A lymphocyte with a flattened nucleus is sticking closely to the foil (the homogeneously stained cell is a platelet).

down before they emerge from the high-*Z* material. Therefore, their track ends, characterized by an elevated LET, will be preferentially located in the nuclei of adjacent cells, so that the RBE for biological effects in these cells will probably be increased. In agreement with observations in CHO-K1 cells by Zellmer *et al.* (*2*), we reported in a previous short communication that an enhancement of RBE was observed for the induction of chromosome aberrations in a monolayer of human T lymphocytes positioned close to the surface of an X-irradiated gold foil, with 2 μm of Mylar in between (*7*). Dicentric chromosomes and acentric fragments, i.e. unstable chromosome anomalies, were taken as models for the oncogenically relevant stable anomalies, the translocations and interstitial deletions. This study has now been complemented by further experiments with the cells either directly attached to the gold surface or with a Mylar spacer with a thickness of 0.9 μm or 2 μm. Dose determinations have been updated by a detailed consideration of the microscopic structure of the lymphocyte monolayer. Here we give a comprehensive report on the enhancement of the RBE as well as of the H ratio, a cytogenetic index of changes in LET (*8*), in the field of the secondary electrons emerging from the gold foil. We explain our results by the elevated values of dose-mean restricted LET near the electron track ends. For additional information, electron spectra and energy deposition data obtained by Monte Carlo simulation of the experiment are considered, and the dose-dependent overdispersion of the intercellular distribution of the chromosome aberration data is interpreted.

MATERIALS AND METHODS

T lymphocytes were obtained from fresh blood samples supplied with informed consent by a 60-year-old healthy male donor. Separation from other blood components was performed by gradient centrifugation in the

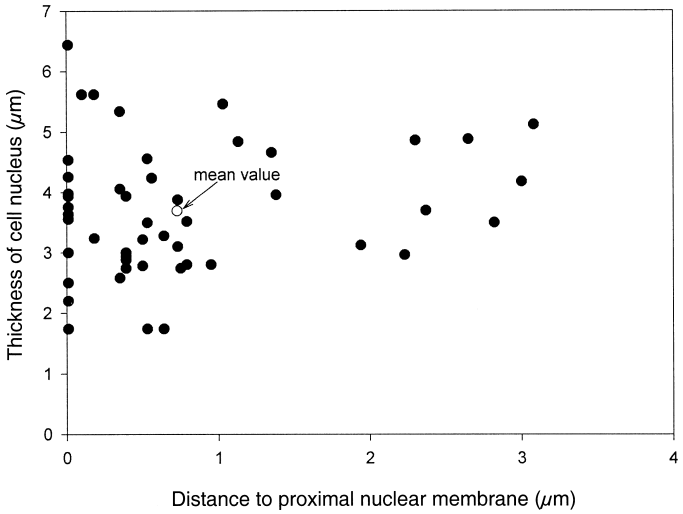

FIG. 2. Scatter diagram of the distance from the carrier foil to the proximal nuclear membrane and of the thickness of the cell nucleus for 50 randomly chosen surface-attached T lymphocytes, stimulated with phytohemagglutinin. Evaluation by optical microscopy.

presence of Lymphoprep™. The lymphocytes were then resuspended in RPMI 1640 medium supplied with 2.5% PHA (phytohemagglutinin) and were pipetted into a dish formed by a 2.5-mm-thick glass ring of 45 mm inner diameter and a stretched Mylar foil (polyethyleneterephthalate, PET) of 0.9 or 2 μm thickness glued to the glass ring. During a 3-h incubation, the cells were allowed to settle as a monocellular layer and to attach to the Mylar foil. An experimental modification was achieved by allowing the cells to settle upon the clean surface of a 150-μm-thick gold foil. Subsequent to the 3-h incubation, the Mylar foil and the gold surface were washed with medium to remove unattached cells.

Transmission electron microscopy was used to study the geometry of cell attachment to the carrier surface. Specimens from sections made perpendicular to the cell layer were rinsed in phosphate-buffered saline (PBS, pH 7.35), prefixed in 1% glutaraldehyde in PBS for 15 min, and postfixed in 2% OsO_4 in PBS for 15 min. In a graded series of ethanol, the samples were dehydrated and embedded in Epon. Ultrathin sections (70–80 nm) were double-stained with uranyl acetate and lead citrate and then examined with a Zeiss EM 10-C electron microscope (Oberkochen, Germany). Typical electron micrographs of the attached cells are shown in Fig. 1. The attached lymphocytes form a single cell layer whose thickness is determined mainly by the cell nuclei.

To examine a statistically representative sample of the attached cells, semithin (1 μm) sections perpendicular to the carrier foil (Ultracut E, Reichert-Jung Leica, Bensheim, Germany) were stained with 1% Toluidine blue for light microscopy. Dehydration of the lymphocytes during preparation may have caused shrinkage in volume of up to 10%. The technique of cell preparation guaranteed that the topological relationships were not altered. Micrographs of sections of 50 cells, selected randomly, were evaluated to obtain accurate values of the geometry of the cell nuclei. The scatter diagram in Fig. 2 shows the characteristic data for each of the 50 cells. The distance between the carrier foil and the proximal nuclear membrane ranged from about 0.01 to 3.0 μm (mean value: 0.73 μm), and the thickness of the cell nuclei ranged from about 2.0 to 5.5 μm (mean value: 3.69 μm).

The dish with the Mylar foil bottom was put into the irradiation position in air facing a horizontal X-ray beam, with the cell layer toward the X-ray source and with a 150-μm gold foil present or absent immediately behind the Mylar foil (Fig. 3 a, c). In the experimental modification without Mylar foil, the gold foil and the cells attached to the gold surface were irradiated in the same geometry (Fig. 3b). The time of X-ray exposure did not exceed 12 min, so that the cells did not dry out. Immediately after irradiation, the cells were scraped off the Mylar or gold foil and were incubated at 37°C with fresh medium containing 2.5% PHA and 2.9 μg/ml BrdU for 48 h, in the presence of 0.1 μg/ml Colcemid during the final 3 h. The microscopic preparations were stained with FPG (fluorescence plus Giemsa) to label the BrdU-marked chromatids, so that selection of first mitoses was possible. Dicentric chromosomes, centric rings and supernumerary acentric fragments (i.e. all acentric fragments minus one per dicentric and per centric ring) were recorded, and the supernumerary acentric fragments were further classified as either interstitial deletions (minutes and larger acentric rings) or linear fragments.

The irradiations were performed in the IAEA/WHO Secondary Standard Dosimetry Laboratory of the GSF Institute of Radiation Protection using 60 kV X rays filtered with 4 mm aluminum and 0.6 mm copper, at an air kerma rate of about 22 mGy min^{-1} at the irradiation position and applying a transmission monitor chamber. The voltage-filtration combination corresponded to the standardized A60 spectrum (*9*), which is confined to the photon energy region 40 to 60 keV and characterized by a mean photon energy of 48 keV. The source–sample distance in air was 50 cm, and the field size in the plane of the cell layer was 10×10 cm^2. A commercial 1-cm^3 ionization chamber type M23361-418, manufactured by Physikalisch-Technische Werkstaetten, Freiburg, Germany, served to measure air kerma K_a at the position of the cells, and the soft tissue kerma at this position was obtained using a conversion factor of 1.02 (*10*). The soft tissue kerma was taken as a good estimate of the absorbed dose in the cells when they were irradiated in the absence of the gold foil (Fig. 3a), because secondary electron equilibrium was provided by the secondary electrons from the air in front and in back of the cell layer and carrier foil. The dose enhancement due to photoelectrons from the glass

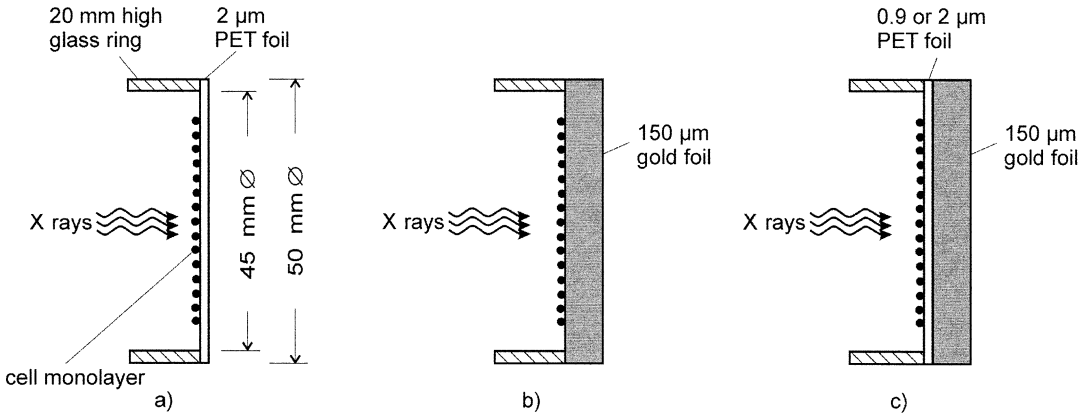

FIG. 3. Scheme of the irradiation geometry for a single cell layer (a) attached to a Mylar carrier foil without gold backing, (b) directly attached to a 150-μm-thick gold foil, or (c) attached to a Mylar carrier foil backed by a 150-μm-thick gold foil.

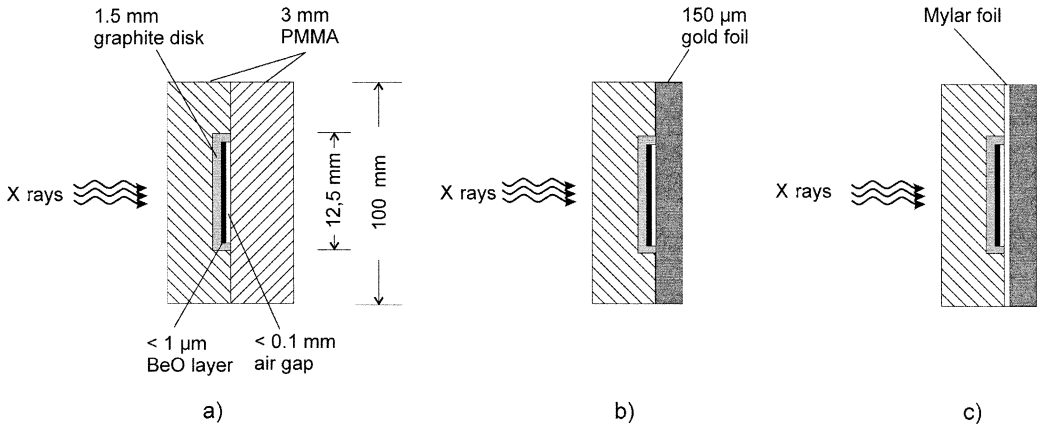

FIG. 4. Scheme of the measurement of the dose enhancement factor DEF using a TSEE dosimeter with a BeO sensor layer on a graphite carrier. The BeO layer recorded the electrons emerging from the entrance surface of either a 3-mm sheet of PMMA (a) or a gold foil (b). A Mylar foil of variable thickness could be inserted between the gold foil and the BeO layer (c).

ring was estimated as negligible; furthermore, its effect would have been in the direction of increasing the observed RBE.

For exposures with the cells directly attached to a 150-μm-thick gold foil (Fig. 3b) or with the gold foil arranged behind the Mylar carrier foil (Fig. 3c), the dose enhancement caused by the secondary electrons emerging from the entrance surface of the gold foil had been measured previously with TSEE (thermally stimulated exo-electron) dosimeters (*1, 3*) as a function of the thickness of the Mylar foil interposed between the gold surface and the sensitive dosimeter layer (Fig. 4a–c). The radiation-sensitive layer of the TSEE detectors consisted of a beryllium oxide (BeO) layer with a thickness of ≤0.1 μm evaporated on a TSEE inactive substrate (graphite). During irradiation, a residual air gap of ≤100 μm remained between the BeO layer and the gold surface. The very thin BeO layer was regarded as a Bragg-Gray cavity sensing the incoming electrons, with spectra as given by the present experiment (Fig. 6) at constant efficiency. The graphite layer, compared to an ideally air-equivalent backing of the BeO layer, was theoretically estimated to reduce the signal in the absence of the gold foil by about 4%. We have neglected this effect because its consideration would have increased the observed RBEs by only 4%.

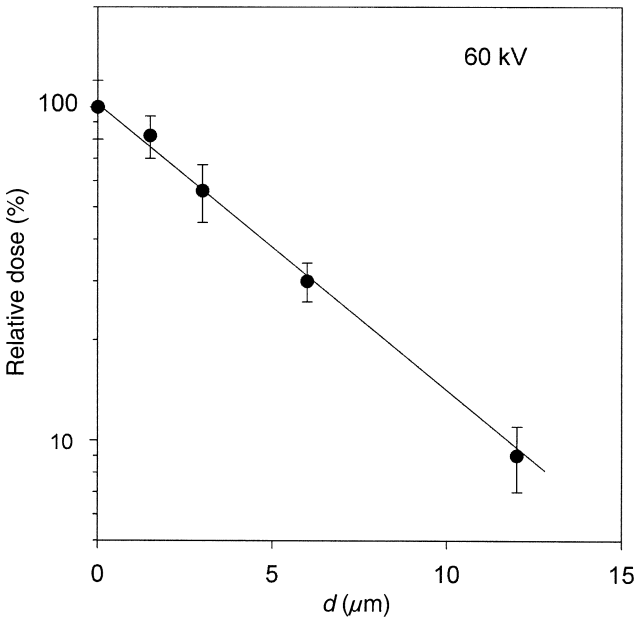

FIG. 5. Relative change in the signal of the BeO sensor in presence of the gold foil, normalized to its signal in the presence of the PMMA sheet with the thickness *d* of a Mylar foil inserted between the gold surface and the BeO sensor. For the experimental arrangement, see the legend to Fig. 4. 60 kV X rays. The straight line was fitted by eye.

The dose enhancement factor, DEF, was obtained as the ratio of the TSEE counts measured with the gold foil (Fig. 4b,c) and with a 3-mm PMMA sheet replacing the gold foil (Fig. 4a). For the present geometry, the maximum DEF was 78 ± 13, and the approximately exponential attenuation curve for the secondary electrons in the Mylar foils was characterized by a 37% thickness of 5 ± 0.1 μm (Fig. 5). Accordingly, the effective attenuation coefficient was 0.196 μm^{-1}. By combining this exponential attenuation curve with the geometric data shown in Fig. 2, we were able to calculate the individual mean absorbed dose to each cell nucleus within the representative sample of 50 cells for the cells directly attached to the gold foil as well as for those separated from it by 0.9- or 2-μm-thick Mylar foils. According to the variations in the shape and position of the cell nuclei (Fig. 2), the relative standard deviation of the individual absorbed doses was 18.9%. The corresponding dose enhancement factors averaged over the 50 representative cells for a given thickness of Mylar foil were 55.7, 46.6 and 37.5 for foil thicknesses of 0, 0.9 and 2.0 μm. Since a 3-mm-thick sheet of PMMA was used to replace the gold foil in the TSEE experiment without gold foil (Fig. 4a), the backscattering factor of this PMMA sheet (1.14) was estimated according to the data of Wachsmann and Drexler (*11*) and was allowed for in the dose calculation. Thus the absorbed doses administered to the cells were $D_1 = 1.02\ K_a$ in the absence of the gold foil and $D_2 = 1.02\ K_a \times 1.14$ DEF in its presence, so that the quotient of these two doses, for the same monitor signal, was $D_2/D_1 = 1.14$ DEF. Since cell preparation for light microscopy may have introduced a volume shrinkage of up to 10%, the D_2 may have been smaller by up to 1.6% on average.

Figure 6 shows the Monte Carlo-calculated spectrum of the secondary electrons emerging from the entrance surface of a plane gold foil exposed to monoenergetic 48 keV photons. Four components of the electron spectrum can be distinguished, namely (from right to left) the M-shell and L-shell photoelectrons and two groups of Auger electrons. Each of these spectral groups is characterized by a maximum energy and by broadening toward lower energies as a consequence of the slowing down of the electrons within the gold foil on their way to the gold surface. The two groups of photoelectrons and the higher-energy Auger electron group will contribute to the radiation exposure of a cell layer directly adjacent to the interface, but the Auger electrons have a maximum energy of about 7 keV and therefore cannot penetrate the 0.9- or 2-μm-thick Mylar foil. This is demonstrated by the calculated depth–dose curve for a layer of water positioned in front of the gold foil (Fig. 7), which shows a detectable contribution from Auger electrons only at depths less than 0.7 μm. In summary, the secondary electrons emerging from the entrance surface

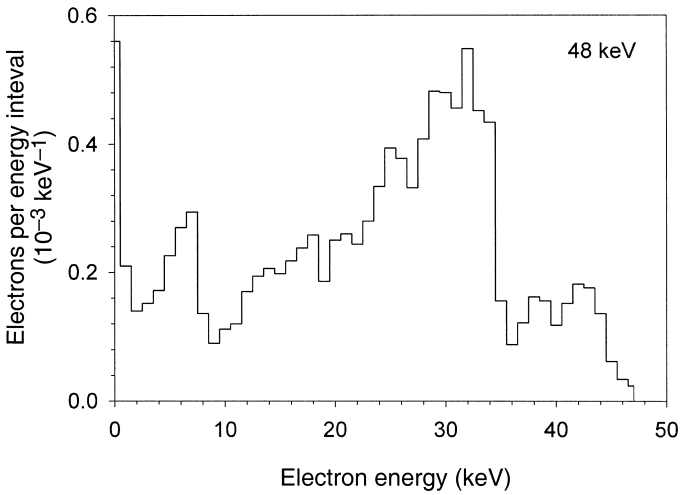

FIG. 6. Monte Carlo-calculated spectral distribution of the number of secondary electrons emerging from the entrance surface a gold foil exposed to 48 keV photons. Peaks (from right to left): M-shell photoelectrons, L-shell photoelectrons, and Auger electrons.

of the gold foil are causing a large dose enhancement in the adjacent lymphocyte layer and, due to the track ends of these electrons within the cell nuclei, are also expected to yield a dose contribution with elevated LET.

The Monte Carlo results referred to in this paper were obtained by simulating the tracks of photoelectrons and Auger electrons and of their further-generation secondary electrons in gold and adjacent water using the PARTRAC code (*12, 13*). Photons and secondary electrons were followed, event by event, throughout the gold foil, using photoionization (*14*), fluorescence and Auger effect data (*15–17*) as well as elastic electron scattering data for gold (*18–20*). Electron histories were terminated at 100 eV. The PARTRAC track structure code allowed us to score the momentary energies of the electrons crossing the interface between gold and tissue. In the energy range considered, the process of photoelectric absorption of photons in different atomic shells of gold is responsible for the production of most of these electrons. The details will be published.

RESULTS

The results of the chromosome analysis of dicentrics, centric rings, interstitial deletions and linear fragments (per 100 surviving cells) are presented in Table 1. For all doses, each of the values is the pooled result of two independent experiments resulting from exposures to 60 kV X rays in the absence or presence of the gold foil. To reduce statistical fluctuations further, the yields of dicentrics and centric rings were pooled to form a combined group, and another combined group was formed from all supernumerary acentric fragments. For these combined groups, the background frequencies of $(0.030 \pm 0.017) \times 10^{-2}$ dicentrics and centric rings per cell and $(0.210 \pm 0.046) \times 10^{-2}$ acentric fragments per cell from the present blood donor are not significantly different from the mean values of $(0.050 \pm 0.007) \times 10^{-2}$ dicentrics and centric rings per cell and $(0.230 \pm 0.016) \times 10^{-2}$ acentric fragments per cell obtained from 141 control individuals (total number of cells 92,550) examined in our laboratory (*8*).

The dose–yield relationships determined for the two

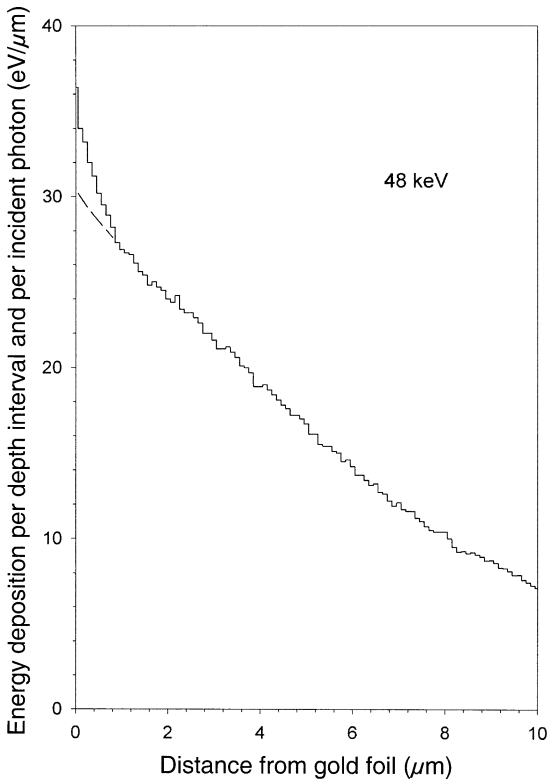

FIG. 7. Monte Carlo-calculated depth–dose curve in water of the secondary electrons emerging from the entrance surface of a gold foil exposed to monoenergetic photons of 48 keV. The dashed curve branch has been drawn by hand for qualitative separation of the small dose contribution by Auger electrons (maximum energy 7 keV) from the prevailing dose contribution by photoelectrons.

combined groups of chromosome aberrations at doses up to 6 Gy are shown in Fig. 8. The error bar attached to each point indicates the standard error of the mean, estimated by repetition of the experiment. Linear-quadratic functions were fitted to the measured points by a maximum-likelihood algorithm, in which their experimental standard deviations were considered. The α values, i.e. the initial slopes of the fitted curves, and the β values, i.e. the coefficients of the dose-squared terms thereby obtained, are presented in Table 2. The stated uncertainties of these values are the standard deviations. (The data in the last line of Table 1, obtained at the highest dose of 7.66 Gy, were excluded from the fit because they fell significantly below the linear-quadratic relationship determined by the yield data for the seven lower doses. Their inclusion would have led to unrealistically high initial slopes.) The two last columns of Table 2 contain the RBE values calculated as quotients of the α values with and without the gold foil, i.e. the ''low-dose RBEs''. The standard deviations associated with the RBE values were calculated according to the error propagation law.

The intercellular distributions of the yield data for the combined groups of aberrations are presented in Tables 3 and 4. In the absence of the gold foil, the distributions show regular dispersion, i.e. a Poisson distribution, since their

TABLE 1
Chromosome Aberration Yields in Human Lymphocytes after Irradiation with 60 kV X Rays in the Absence or Presence of Secondary Electrons Released from a Gold Foil

				Chromosome aberrations per 100 cells					
Gold foil (150 μm)	Mylar foil (μm)	Dose (Gy)	Cells scored	Dicentrics	Centric rings	Interstitial deletions	Linear fragments	Dicentrics and rings	Acentric fragments
Without	2.0	0.000	10000	0.03	0	0.02	0.19	0.03	0.21
Without	2.0	0.051	2500	0.32	0.04	0.04	0.36	0.36	0.40
Without	2.0	0.102	1500	0.73	0.07	0.07	0.93	0.80	1.00
Without	2.0	0.204	3000	0.97	0.10	0.20	1.20	1.07	1.40
Without	2.0	0.510	2500	2.64	0.24	0.44	2.76	2.88	3.20
Without	2.0	1.020	700	6.71	0.71	1.43	6.86	7.42	8.29
Without	2.0	1.530	700	12.0	1.57	1.57	13.71	13.57	15.28
With	0.0	0.557	500	4.6	0.4	1.0	5.4	5.0	6.4
With	0.0	1.114	300	11.7	1.3	2.7	9.0	13.0	11.7
With	0.0	1.726	500	18.8	1.8	3.8	12.8	20.6	16.6
With	0.0	2.840	400	46.3	4.8	8.5	27.3	51.1	35.8
With	0.0	4.065	300	68.7	7.3	18.0	47.3	76.0	65.3
With	0.0	5.879	200	119.0	12.0	29.0	79.5	131.0	109.5
With	0.9	0.466	500	4.4	0	1.2	4.2	5.0	5.4
With	0.9	0.931	300	9.7	1.0	2.7	5.7	10.7	8.4
With	0.9	1.443	400	13.8	1.3	3.0	18.3	15.1	21.3
With	0.9	2.374	500	42.0	3.2	4.2	30.0	45.2	34.2
With	0.9	3.306	200	52.0	6.0	17.5	41.0	58.0	58.5
With	0.9	4.749	300	100.0	9.7	25.0	68.3	109.7	93.3
With	2.0	0.375	200	4.0	1.0	1.0	2.5	5.0	3.5
With	2.0	0.751	300	6.7	0.7	1.7	5.3	7.4	7.0
With	2.0	1.164	200	7.5	1.0	1.5	6.5	8.5	8.0
With	2.0	1.915	500	19.2	2.4	5.0	18.6	21.6	23.6
With	2.0	2.665	300	29.0	3.7	7.0	21.3	32.7	28.3
With	2.0	3.830	300	63.3	7.0	14.0	60.0	70.3	74.0
With	2.0	5.632	100	83.0	7.0	20.0	64.0	90.0	84.0
With	2.0	7.660	200	110.0	9.5	24.5	91.0	119.5	115.5

Notes. The stated absorbed dose is D_1 for irradiations without gold foil and D_2 for irradiations with gold foil (see text). For irradiations with gold foil, Mylar foils 0, 0.9 or 2 μm thick were inserted between the cell layer and the gold surface. The last two columns represent aberration yields pooled from dicentrics and centric rings, respectively, from interstitial deletions and linear fragments.

dispersion coefficients σ^2/y (variance/mean) are close to 1. In presence of the gold foil, the distributions are generally overdispersed as σ^2/y differs from value 1. The significance of the observed excess of σ^2/y over 1 is assessed in terms of the test quantity u, and values of u in excess of 1.96 indicate overdispersion at the 5% level of significance. There is an overall increase in the dispersion coefficient σ^2/y with increasing dose.

We also determined the H ratio, the quotient of the yields of the interstitial deletions and of the dicentrics pooled over all doses. The H value in the absence of the gold foil was 0.169 ± 0.027 (45 interstitial deletions, 265 dicentrics), and for exposures in the presence of the gold foil, we obtained $H = 0.228 \pm 0.019$ (178 interstitial deletions, 781 dicentrics) when the cells were immediately attached to the gold foil, $H = 0.212 \pm 0.019$ (157 interstitial deletions, 742 dicentrics) with the 0.9-μm Mylar foil, and $H = 0.232 \pm 0.020$ (167 interstitial deletions, 719 dicentrics) with the 2-μm Mylar foil inserted between the cell layer and the gold foil. The three H values with the gold foil present are not significantly different from each other, and their average is 0.224 ± 0.011.

DISCUSSION

The first point to be discussed is the secondary electron field to which the lymphocytes are exposed during their irradiation free in air (Fig. 3a). The source of these electrons is the air between the monitor chamber of the X-ray apparatus and the cell layer. At 48 keV of photon energy, only about 10% of the secondary electrons produced in air are the photoelectrons from nitrogen and oxygen, and 90% are Compton electrons. However, the maximum energy of the Compton electrons (7.6 keV) and therefore their maximum range in air (about 0.9 mm) is small compared to the range of the photoelectrons (about 36 mm) so that more than 80% of the electron fluence at a given point of interest in a broad X-ray beam consists of photoelectrons. From a narrow X-ray beam with a radius comparable to the range of the photoelectrons, part of them would escape to the side by scattering and convection. But in the present case, for a field size of 10×10 cm^2, this escape had a negligible influence, so that during irradiations free in air the cells were irradiated with a fluence of secondary electrons produced in air, built up to its equilibrium value. This ''inci-

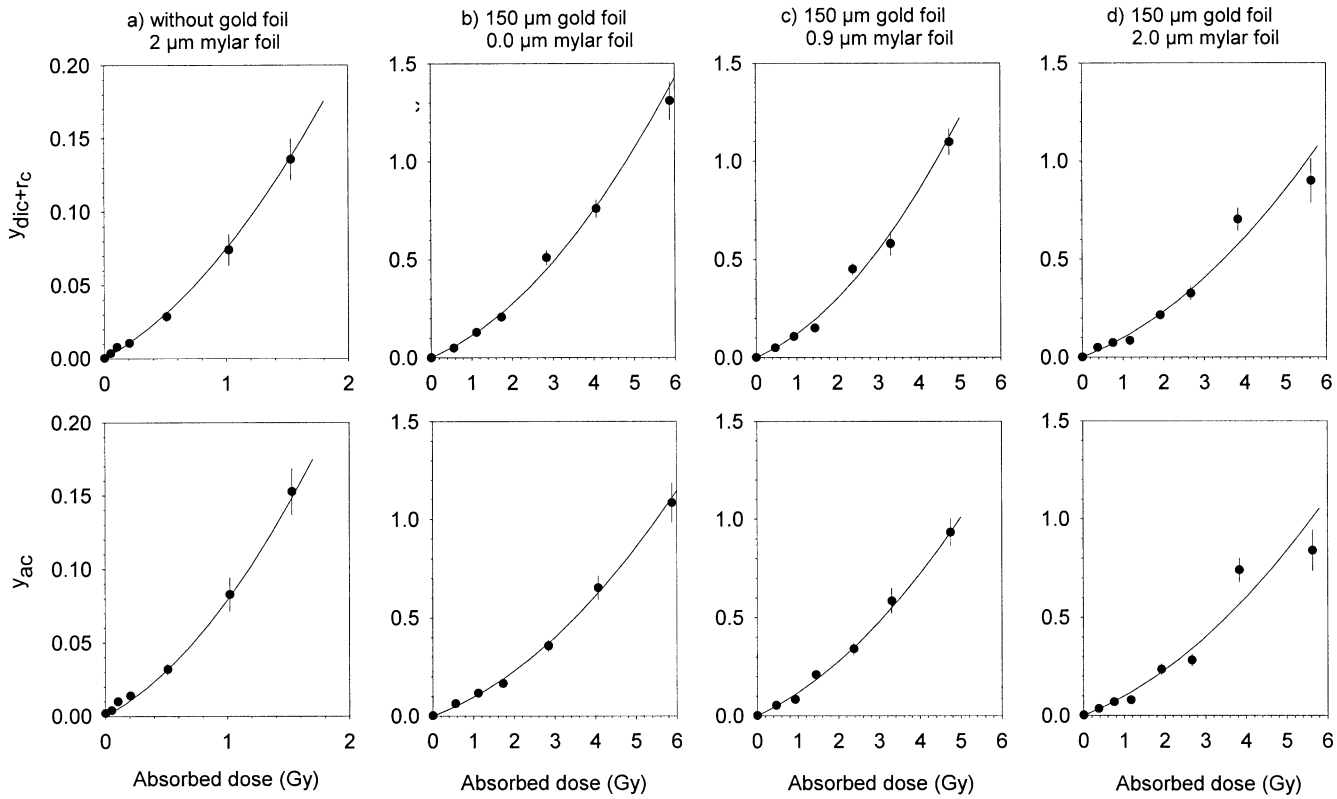

FIG. 8. Experimental dose–effect data and linear-quadratic fitting curves for dicentrics, dic, and centric rings, r_c (upper panels), and for supernumerary acentric fragments (lower panels). Ordinate values: yields per surviving cell. Irradiation geometry (a) without gold foil, with 2-µm Mylar foil (see Fig. 3a); (b) with gold foil, 0-µm Mylar foil (see Fig. 3b); (c) with gold foil, 0.9-µm Mylar foil (see Fig. 3c); (d) with gold foil, 2-µm Mylar foil (see Fig. 3c).

dent'' component of the radiation field remains essentially unchanged when a gold foil is positioned behind the cell layer, being merely modified by the change in electron backscattering. However, the main components of radiation to which the cells are now exposed are the photoelectrons and Auger electrons emerging from the entrance surface of the gold foil into the upstream half-space (Fig. 3b, c).

The linear-quadratic shape of the dose–yield curves (Fig. 8) corresponds to the results obtained with the same surface-attached lymphocytes in studies with ^{137}Cs γ radiation (*21*) and 10 kV X rays (*22*).

To understand the increase in the α coefficient for exposures in the presence of the gold foil compared to exposures in its absence (Table 2), we must consider that the dose contributed by the secondary electrons emerging from the gold foil decreases by a factor of about two across the volume of a cell nucleus (Fig. 5). This means that about 50% of the electrons entering a cell nucleus are stopped within the nuclear volume, and that their track ends are preferentially located in the region immediately behind the proximal nuclear membrane. On the other hand, exposures without gold foil are characterized by an equilibrium spectrum of secondary electrons at each point of interest in the cells; they comprise a smaller number of electron track ends per unit of dose, and these track ends have no local preference. Since electron track ends are characterized by ele-

TABLE 2
Dose–Yield Coefficients α ± SD, β ± SD, and Derived RBE ± SD for Chromosome Aberrations in Human Lymphocytes after Irradiation with 60 kV X Rays in the Absence or Presence of Secondary Electrons Released from a Gold Foil

Gold foil 150 µm	Mylar foil (µm)	Dicentrics and centric rings		Acentric fragments		RBE	
		α (Gy^{-1})	β (Gy^{-2})	α (Gy^{-1})	β (Gy^{-2})	Dicentrics and centric rings	Acentric fragments
Without	2.0	0.047 ± 0.008	0.028 ± 0.010	0.045 ± 0.013	0.034 ± 0.014		
With	0.0	0.088 ± 0.012	0.025 ± 0.003	0.074 ± 0.011	0.020 ± 0.003	1.87 ± 0.41	1.71 ± 0.55
With	0.9	0.089 ± 0.013	0.031 ± 0.004	0.098 ± 0.013	0.022 ± 0.004	1.89 ± 0.42	2.16 ± 0.68
With	2.0	0.081 ± 0.012	0.018 ± 0.004	0.083 ± 0.015	0.017 ± 0.003	1.73 ± 0.39	1.84 ± 0.63

TABLE 3
Intercellular Distributions of the Number of Dicentric Chromosomes plus Centric Rings in Human Lymphocytes after Irradiation with 60 kV X Rays, in the Absence or Presence of Secondary Electrons Released from a Gold Foil

Dose (Gy)	Cells scored	Distribution									σ^2/y	*u* value
		0	1	2	3	4	5	6	7	8		
Without gold												
0.051	2500	2491	9								1.00	−0.11
0.102	1500	1488	12								0.99	−0.21
0.204	3000	2969	30	1							1.05	1.97
0.510	2500	2431	66	3							1.06	2.14
1.020	700	652	44	4							1.08	1.51
1.530	700	616	74	9	1						1.12	2.26
With gold, 0.0-μm Mylar foil												
0.557	500	477	21	2							1.11	1.77
1.114	300	265	31	4							1.08	0.98
1.726	500	416	67	15	2						1.20	3.24
2.840	400	248	106	41	4	1					1.07	1.01
4.065	300	158	82	37	20	3					1.25	3.06
5.679	200	69	55	45	18	7	3	2	0	1	1.44	4.40
With gold, 0.9-μm Mylar foil												
0.466	500	476	23	1							1.03	0.48
0.931	300	269	30	1							0.96	−0.55
1.443	400	344	52	4							0.99	−0.20
2.374	500	327	127	41	3	2					1.10	1.58
3.306	200	115	62	17	4	2					1.27	2.70
4.749	300	120	83	58	29	8	1	1			1.23	2.82
With gold, 2.0-μm Mylar foil												
0.375	200	191	8	1							1.16	1.68
0.751	300	279	20	1							1.03	0.33
1.164	200	185	13	2							1.16	1.65
1.915	500	412	72	15	2						1.18	2.86
2.665	300	225	52	23							1.15	1.84
3.830	300	284	56	42	16	1	1				1.42	5.15
5.632	100	51	21	19	6	2	1				1.43	3.04
7.660	200	110	41	29	21	9	7	1			1.72	7.20

vated LET values, the enhancement of the coefficient for exposures in the presence of the gold foil can therefore be explained qualitatively by an increase in the number of electron track ends per unit of dose.

For quantitative interpretation of the observed RBE values, varying from about 1.7 to about 2.1 (Table 2), the dose-mean restricted linear energy transfer, $L_{500,D}$, can serve as a suitable microdosimetric parameter, because systematic evaluations of the yields of dicentric chromosomes in human lymphocytes exposed to electrons, photons, protons and neutrons have shown that the coefficient α_{dic} is approximately proportional to the $L_{500,D}$ values associated with these radiations (*23*). In calculations of restricted linear energy transfer, the LET values of the ''track core'' and of the secondary electrons with initial kinetic energies exceeding 500 eV are considered separately. This separation into components corresponds to the geometry of a DNA target such as the 30-nm chromatin fiber which, if hit by the track core, is essentially not hit by the far-reaching secondary electrons. Dose weighting of parameter L_{500} is applied because the product $\alpha \times D$ determines the aberration yield and α varies in proportion to L_{500}.

Calculations of $L_{500,D}$ values for electron tracks with various initial energies have been performed by Blohm.[2] For instance, the photoelectrons from silver characteristic L-shell radiation, with a most probable energy of 3.15 keV, which have an $L_{500,D}$ of 12.4 keV/μm, can be taken as grossly representative for the photoelectrons and Auger electrons irradiating the lymphocytes, providing the above-mentioned large dose contribution due to electron track ends in the cell nuclei. On the other hand, the secondary electrons released in air by 48 keV photons have an $L_{500,D}$ of about 6.6 keV/μm. The quotient of these two $L_{500,D}$ values is 1.88. We can therefore, in a gross approximation, explain the observed RBE values, which range from 1.7 to 2.1 (Table 2), by referring to the above-mentioned proportionality of

[2] R. Blohm, Passage of electrons through radiation sensitive regions of the cell nucleus. Thesis, University of Göttingen, Germany, 1983. [in German]

TABLE 4
Intercellular Distributions of the Number of Acentric Fragments in Human Lymphocytes after Irradiation with 60 kV X Rays in the Absence or Presence of Secondary Electrons Released from a Gold Foil

Dose (Gy)	Cells scored	Distribution									σ^2/y	u value
		0	1	2	3	4	5	6	7	8		
Without gold												
0.051	2500	2490	10								1.00	−0.15
0.102	1500	1486	13	1							1.12	3.40
0.204	3000	2960	38	2							1.11	4.31
0.510	2500	2425	71	3	1						1.12	4.27
1.020	700	650	42	8							1.19	3.58
1.530	700	608	77	15							1.13	2.44
With gold, 0.0-μm Mylar foil												
0.557	500	469	30	1							1.00	0.01
1.114	300	267	31	2							1.00	−0.01
1.726	500	433	52	14	1						1.25	3.97
2.840	400	293	80	20	5	2					1.30	4.25
4.065	300	182	72	30	7	5	2	1	1		1.75	9.19
5.679	200	95	47	29	15	6	5	1	2		1.90	12.73
With gold, 0.9-μm Mylar foil												
0.466	500	475	23	2							1.10	1.61
0.931	300	277	22	0	1						1.17	2.06
1.443	400	327	60	11	1						1.12	1.70
2.374	500	368	98	16	8	3	1				1.46	7.22
3.306	200	122	50	22	3	1	2				1.40	4.00
4.749	300	144	83	45	12	12	2	1	1		1.57	6.98
With gold, 2.0-μm Mylar foil												
0.375	200	193	7								0.97	−0.32
0.751	300	281	17	2							1.12	1.55
1.164	200	184	16								0.93	−0.77
1.915	500	410	65	22	3						1.67	10.63
2.665	300	234	48	17	1						1.19	2.24
3.830	300	164	80	36	14	4	1	0	1		1.55	6.74
5.632	100	47	34	10	6	3					1.27	1.91
7.660	200	76	68	30	9	11	4	2			1.47	4.70

the α values with $\bar{L}_{500,D}$. At distances from the gold surface exceeding the maximum range of the emitted photoelectrons, the enhancements of dose and RBE are expected to cease, leaving only a small dose enhancement due to photon backscattering from the gold foil.

Figure 9 shows the $\bar{L}_{500,D}$ dependence of the H ratio (yield ratio of interstitial deletions and dicentrics) for lymphocytes cultured and examined in the same way as in the present paper. This dependence was determined empirically with ^{137}Cs γ radiation (*21*), 10 kV X rays (*22*) and 5 MeV α particles (*21*). The H ratio is representative of the yield ratio of intra- and interchromosomal exchange-type aberrations and can be regarded as a ''fingerprint'' of radiation quality. The elevated $\bar{L}_{500,D}$ associated with electron track ends should be noticeable when the H values resulting from the present experiment are entered into this plot. The data in Fig. 9 show that when the H values of 0.169 ± 0.027 and 0.224 ± 0.011 observed in the experiments without and with gold foil are positioned on the fitting line, the corresponding abscissa readings are 10.5 ± 2 keV/μm and 18.5 ± 2 keV/μm, and their quotient is 1.76 ± 0.4. The evaluation of the observed H ratios therefore again suggests that the RBE enhancement for chromosome aberrations induced by secondary electrons emerging from a gold foil is caused by the elevation of LET due to the track ends of the secondary electrons within the lymphocyte nuclei.

In our preliminary communication (*7*), we reported somewhat smaller α and β values for irradiations in the presence of the gold foil, because the dose determination in our previous study (*7*) had assumed that each cell nucleus was extended over a range of exactly 0 to 3 μm from the carrier foil. This estimate has now been corrected using the more realistic data on the geometry of the attached cells (Figs. 1 and 2), yielding dose enhancement factors smaller by about 17%. The α and β values were accordingly increased. From a general viewpoint, we should also mention that the α values shown in Table 2 for irradiations with 60 kV X rays without and with the gold foil can be compared with the α values obtained previously for ^{137}Cs γ radiation with flattened lymphocytes from the same donor (*21*). These values were $\alpha_{dic} = 0.016$ Gy^{-1} for dicentrics (or $\alpha_{dic+rc} = 0.018$ Gy^{-1} when corrected for centric rings) and $\alpha_{ac} = 0.019$ Gy^{-1} for acentric fragments. In comparison with these, the α values from Table 2 are higher by a factor

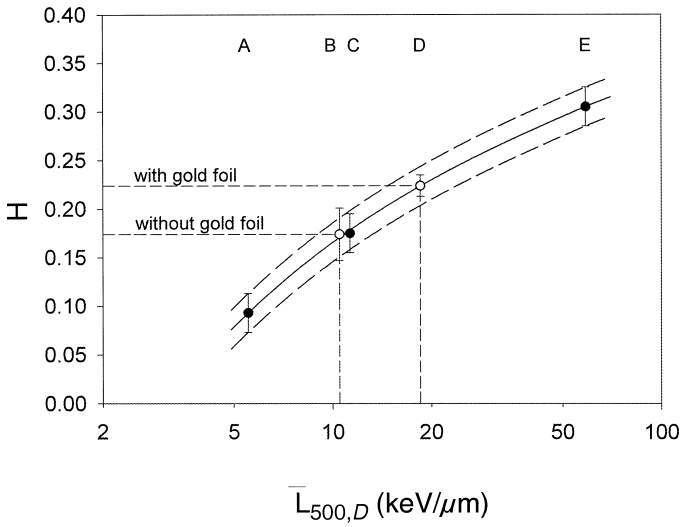

FIG. 9. Plot of the H ratio (yield ratio of interstitial deletions and dicentrics) as a function of dose-mean restricted LET. Full circles: data taken from refs. (*13*) and (*14*) from which the interpolation line and the 95% confidence limits (dashed lines) were generated. Open circles: H values from this paper without gold foil (H = 0.169 ± 0.027) and with gold foil (H = 0.224 ± 0.011), positioned on the interpolation line so that abscissa values can be read off.

of about 2.5 without the gold foil and of about 5 with the gold foil. Such relatively large variations of the ''low-dose RBE'' between different low-LET radiations are a general phenomenon; this has been discussed in the context of radiation protection (*24*).

Finally, to understand the reason for the dose-dependent overdispersion of the intercellular distributions of the aberration number (Table 4), it is helpful to remember that, for lymphocytes from the same donor and subjected to the same preparation techniques, irradiations with homogeneous dose distributions such as with ^{137}Cs γ rays (*21*) or 10 kV X rays (*22*) had given regular dispersion, i.e. Poisson distributions of the numbers of aberrations. Consistent with this experience, we see from Table 4 that exposures without gold foil have resulted in regular dispersion. However, in the presence of the gold foil, the radiation field of the emerging photoelectrons in the adjacent low-*Z* medium is inhomogeneous, as shown in Figs. 5 and 7. Since the dose imparted by the secondary electrons decreases exponentially with a 37% depth of 5 μm, the mean dose received by a cell nucleus (a) will decrease with increasing distance of the proximal nuclear membrane from the carrier foil and (b) will depend on the degree of cell flattening, with the more flattened cells receiving a larger mean nuclear dose than the less flattened cells (see Figs. 1 and 2). This intercellular variation of the mean nuclear dose will result in overdispersion of the chromosome aberrations as shown by a simple example: Consider a mixture of three equally frequent classes of cells with mean values m, $m(1 + a)$ and $m(1 - a)$ of the aberration number per cell (with $0 < a < 1$). If in each class, the aberration number is Poisson distributed, the combination of the three classes gives a new distribution of aberration number n with mean value $\bar{n} = m$, but with variance $\overline{n^2} - \bar{n}^2 = m + 2m^2 \times a^2/3$ and relative variance $1 + 2m \times a^2/3$. This demonstrates that in an inhomogeneous radiation field, the overdispersion should increase with m, i.e. with dose.

However, here is no need to assume that the overdispersion shown in Table 4 should be an LET effect. The overdispersion which can be observed e.g. after α particle irradiation of the same type of cells (*21*) is due to the statistical variation of the number of aberrations caused by the traversal of a single α particle across the cell nucleus in addition to the statistical variation of the number of these traversals (*25*). In view of the shortness of the electron track ends, such multiplicity of the number of aberrations associated with a single particle traversal is not to be expected.

CONCLUSION

The present experiments have shown that the yield of chromosome aberrations in human lymphocytes exposed to the photoelectrons and Auger electrons emerging from the entrance surface of an X-irradiated high-*Z* material reflects not only a localized dose enhancement caused by the release of secondary electrons from this material, but also the expected RBE increase due to the slowed-down spectrum of these particles. RBE values ranging from about 1.7 to about 2.1 with standard deviations of about 0.5 have been observed experimentally, using chromosome aberrations in surface-attached human lymphocytes positioned close to an X-irradiated gold foil as the biological end point. In the strongly inhomogeneous radiation field of the secondary electrons, cell nuclei are hit by an increased number of electron track ends whose elevated values of restricted linear energy transfer result in elevated RBE values in addition to dose enhancement. The LET-dependent cytogenetic parameter H (yield ratio of interstitial deletions and dicentrics) also showed a significant increase when the lymphocytes were exposed in the presence of the photoelectrons and Auger electrons emerging from gold compared to irradiations in their absence. These results agree with the findings of Zellmer *et al.* (*2*), who used the survival of CHO-K1 cells as the end point. We conclude that, wherever secondary electrons will emerge across a low-*Z*/high-*Z* interface in the human body, not only a strong dose enhancement, but also an increase of the RBE for LET-sensitive biological end points will occur in the cell layers lining the interface. This dose and RBE enhancement near the surfaces of high-*Z* materials can be important in considerations of radiation risk to bone marrow and bone-lining cells as well as to cells adjacent to artificial low-*Z*/high-*Z* interfaces.

ACKNOWLEDGMENTS

The authors express their sincere gratitude for valuable assistance to Mrs. U. A. Fill, P. Gais, Mrs. M. Haney, L. Hieber and Mrs. K. Peters, all from the GSF National Research Center.

Received: December 11, 2001; accepted: May 7, 2002

REFERENCES

1. D. F. Regulla, L. B. Hieber and M. Seidenbusch, Physical and biological interface dose effects in tissue due to X-ray-induced release of secondary radiation from metallic gold surfaces. *Radiat. Res.* **150**, 92–100 (1998).
2. D. L. Zellmer, J. D. Chapman, C. C. Stobbe, F. Xu and I. J. Das, Radiation fields backscattered from material interfaces: I. Biological effectiveness. *Radiat. Res.* **150**, 406–415 (1998).
3. D. Regulla, L. Hieber and M. Seidenbusch, The dose enhancement effect at interfaces between tissues and media of higher atomic number: Physical and biological effects in the range of X-ray diagnosis. *Z. Med. Phys.* **10**, 52–62 (2000). [in German]
4. F. W. Spiers, Dosage in irradiated soft tissues and bone. *Br. J. Radiol.* **25**, 365–370 (1951).
5. W. Gössner, R. Masse and J. W. Stather, Cells at risk for dosimetric modelling relevant to bone tumour induction. *Radiat. Prot. Dosim.* **92**, 209–213 (2000).
6. E. A. Nekolla, M. Kreisheimer, A. M. Kellerer, M. Kuse-Isingschulte, W. Gössner and H. Spiess, Induction of malignant bone tumors in radium-224 patients: Risk estimates based on the improved dosimetry. *Radiat. Res.* **153**, 93–103 (2000).
7. D. Regulla, W. Panzer, E. Schmid, G. Stephan and D. Harder, Detection of elevated RBE in human lymphocytes exposed to secondary electrons released from X-irradiated metal surfaces. *Radiat. Res.* **155**, 744–747 (2001).
8. M. Bauchinger and E. Schmid, LET dependence of yield ratios of radiation-induced intra- and interchromosomal aberrations in human lymphocytes. *Int. J. Radiat. Biol.* **74**, 17–25 (1998).
9. ISO Standard 4037-1, X and gamma reference radiations for calibrating dosemeters and doserate meters and for determining their response as a function of photon energy. International Organisation of Standards, Geneva, 1996.
10. ICRU, *Photon, Electron, Proton and Neutron Interaction Data for Body Tissues*. Report 46, International Commission on Radiation Units and Measurements, Bethesda, MD, 1992.
11. F. Wachsmann and G. Drexler, *Graphs and Tables for Use in Radiology*. Springer-Verlag, Berlin and Heidelberg, 1956.
12. H. G. Paretzke, Radiation track structure. In *Kinetics of non-Homogeneous Processes* (G. R. Freeman, Ed.), pp. 89–170. Wiley, New York, 1987.
13. W. Friedland, P. Jacob, H. G. Paretzke and T. Stork, Monte Carlo simulation of the production of short DNA fragments by low-linear energy transfer radiation using higher-order DNA models. *Radiat. Res.* **150**, 170–182 (1998).
14. S. T. Perkins and D. E. Cullen, *ENDL Type Formats for the LLNL Evaluated Atomic Data Library (EADL), for the Evaluated Electron Data Library (EEDL) and for the Evaluated Photon Data Library (EPDL)*. UCRL-ID-117796, Lawrence Livermore National Laboratory, Livermore, CA, 1994.
15. J. H. Hubbel, P. N. Trehan, N. Singh, B. Chand, M. L. Garg, R. R. Garg, S. Singh and S. Pun, A review, bibliography and tabulation of K, L, and higher atomic shell X-ray fluorescence yields. *J. Phys. Chem. Ref. Data* **23**, 339–363 (1994).
16. S. Puri, D. Mehta, B. Chand, N. Singh, J. H. Hubbel and P. N. Trehan, Production of L_i subshell and M shell vacancies following inner-shell vacancy production. *Nucl. Instrum. Methods Phys. Res. B* **83**, 21 (1993).
17. S. Singh, D. Mehta, R. R. Garg, S. Kumar, M. L. Garg, N. Singh, P. C. Mangal, J. H. Hubbel and P. N. Trehan, Average L-shell fluorescence yields for elements $56 < Z < 92$. *Nucl. Instrum. Methods Phys. Res. B* **51**, 5 (1990).
18. S. M. Seltzer, Cross sections for bremsstrahlung production and electron impact ionization. In *Monte Carlo Transport of Electrons and Photons* (T. M. Jenkins, W. R. Nelson and A. Rindi, Eds.), pp. 81–114. Plenum Press, New York, 1988.
19. M. Fink and A. C. Yates, Theoretical electron scattering amplitudes and spin polarizations. *At. Data* **1**, 385 (1970).
20. M. E. Riley, T. MacCallum and E. Biggs, Electron-atom elastic scattering. *At. Data Nucl. Data Tables* **15**, 443–475 (1975); Erratum, *At. Data Nucl. Data Tables* **28**, 379 (1983).
21. E. Schmid, L. Hieber, U. Heinzmann, H. Roos and A. M. Kellerer, Analysis of chromosome aberrations induced by *in vitro* α-particle irradiation. *Radiat. Environ. Biophys.* **35**, 179–184 (1996).
22. H. Roos and E. Schmid, Analysis of chromosome aberrations in human lymphocytes induced by 5.4 keV X-rays. *Radiat. Environ. Biophys.* **36**, 251–254 (1998).
23. D. Harder, Characteristics of electron tracks in matter. In *Radiation Research*, Vol. 2 (M. Moriarty, C. Mothersill, C. Seymour, M. Edington, J. F. Ward and R. J. M. Fry, Eds.), pp. 111–114. Allen Press, Lawrence, KS, 2000.
24. D. Harder, D. Regulla, E. Schmid and D. Frankenberg, Does the LET dependence of the RBE of sparsely ionizing radiations have a meaning in radiation protection? *Strahlenschutzpraxis* **2**, 23–31 (2001). [in German]
25. R. Greinert and D. Harder, Biophysical analysis of the dose dependent overdispersion and the restricted linear energy transfer dependence expressed in dicentric chromosome data from alpha particle irradiated human lymphocytes. *Radiat. Environ. Biophys.* **36**, 89–95 (1997).